Van Hove Function for Diffusion in Zeolites

Martin Gaub,[†] Siegfried Fritzsche,[†] Reinhold Haberlandt,*[,†] and Doros N. Theodorou[‡]

Fakultät für Physik und Geowissenschaften, Universität Leipzig, Linnéstrasse 5, D-04103 Leipzig, Germany, Department of Chemical Engineering, University of Patras, GR-26500 Patras, Greece, and Molecular Modelling of Materials Group, National Research Centre for the Physical Sciences "Demokritos", GR-15310 Ag. Paraskevi, Athens, Greece

Received: October 26, 1998; In Final Form: March 4, 1999

An approximation for the self-part of the van Hove function is derived. The self-part of the van Hove function is calculated by MD simulation for the diffusion of methane in ZK4 and silicalite and compared with the approximation. Fourier transform in space of the van Hove function yields the intermediate scattering function, the decay of which is used to determine the self-diffusion coefficient. Fourier transform in time yields the dynamic structure factor which can be compared with quasi-elastic neutron scattering results.

Introduction

Because of the great importance of zeolites as cracking catalysts, there is much interest in understanding the processes of molecular motion of hydrocarbons in their pores and channels.[1,2] For more than two decades, computer simulations have been used to get insight into the diffusive behavior in zeolites (see refs 3 and 4 for a review). Diffusion coefficients can be obtained from molecular dynamics simulations in several ways.[1,5] The most common methods are based on the determination of the mean square displacement (MSD) and the velocity autocorrelation function, the two being mathematically equivalent. Alternatively, one can explicitly determine the propagator of the motion which is closely related to the density autocorrelation function known as the van Hove function. This is done in the present paper for the diffusion of methane in zeolites. Two different crystals are investigated: the aluminium-free member of the A-type family denoted by ZK4, and the aluminium-free form of ZSM-5, known as silicalite. Moreover, the van Hove function can be Fourier transformed to give the dynamic structure factor which can be compared with experimental results from quasielastic neutron scattering. This is also part of the present work.

The paper is organized as follows: After a short outline of the theoretical basis, we derive an approximation formula for the self-part of the van Hove function. The presentation of results from MD simulations starts with the van Hove function, including a test of our approximation. The intermediate scattering function is shown, and its long-wave limit is used to calculate self-diffusion coefficients. The dynamic structure factor is also shown. Finally, the radially dynamic structure factor is calculated and compared with the quasielastic neutron scattering results.

Theory

Definition of *G*, *F*, and *S* and Separation into Self- and Distinct-Parts. The van Hove function $G(\mathbf{r}, t)$ is defined as the inverse Fourier transform with respect to both space and time of the dynamic structure factor $S(\mathbf{k}, \omega)$, as a generalization of the static case in which the differential cross-section is expressed in terms of the pair correlation function.[6] Conversely,

$$S(\mathbf{k}, \omega) = \frac{1}{2\pi} \int_{-\infty}^{\infty} \int G(\mathbf{r}, t) \exp\{-i(\mathbf{kr} - \omega t)\} \mathrm{d}^3 r \, \mathrm{d}t \quad (1)$$

The intermediate scattering function $F(\mathbf{k}, t)$ is

$$F(\mathbf{k}, t) = \int G(\mathbf{r}, t) \exp\{-i\mathbf{kr}\} \mathrm{d}^3 r \quad (2)$$

Together with Born's scattering formula for $S(\mathbf{k}, \omega)$, the van Hove function for a system of N molecules (whether in a zeolite or not doesn't matter at this stage) reads[6]

$$G(\mathbf{r}, t) = \frac{1}{N} \left\langle \sum_{j=1}^{N} \sum_{l=1}^{N} \int \delta[\mathbf{r} + \mathbf{r}_l(0) - \mathbf{r}'] \delta[\mathbf{r}' - \mathbf{r}_j(t)] \, \mathrm{d}^3 r' \right\rangle \quad (3)$$

where $\mathbf{r}_j(t)$ is the center-of-mass position of molecule j at time t. One easily recognizes the number density $\rho(\mathbf{r}, t) = \sum_{j=1}^{N} \delta(\mathbf{r} - \mathbf{r}_j(t))$. Setting $\mathbf{r}'' = \mathbf{r}' - \mathbf{r}$, we can rewrite eq 3 as

$$G(\mathbf{r}, t) = \frac{1}{N} \int \langle \rho(\mathbf{r}'', 0) \rho(\mathbf{r}'' + \mathbf{r}, t) \rangle \, \mathrm{d}^3 r'' \quad (4)$$

So, $G(\mathbf{r}, t)$ can be interpreted as the homogenized, normalized autocorrelation function of the number density. If quantum effects can be neglected, all operators r_l commute in eq 3, yielding

$$G(\mathbf{r}, t) = \frac{1}{N} \left\langle \sum_{j=1}^{N} \sum_{l=1}^{N} \delta[\mathbf{r} + \mathbf{r}_l(0) - \mathbf{r}_j(t)] \right\rangle \quad (5)$$

This is seen to be the probability density of finding some particle at time t at distance $\mathbf{r}$ from the position of a particle at time 0. For particles that can be regarded as distinguishable, it is natural to split the function as follows:

$$G(\mathbf{r}, t) = G_s(\mathbf{r}, t) + G_d(\mathbf{r}, t) \quad (6)$$

* To whom correspondence should be addressed: Reinhold.Haberlandt@physik.uni-leipzig.de.
[†] Universitat Leipzig.
[‡] University of Patras.

10.1021/jp984177f CCC: $18.00
Published on Web 05/14/1999

$$G(\mathbf{r}, t) = \frac{1}{N}\left\langle \sum_{j=1}^{N} \delta[\mathbf{r} + \mathbf{r}_j(0) - \mathbf{r}_j(t)] \right\rangle \tag{7}$$

$$G_d(\mathbf{r}, t) = \frac{1}{N}\left\langle \sum_{j=1}^{N} \sum_{l=1}^{N} \delta[\mathbf{r} + \mathbf{r}_l(0) - \mathbf{r}_j(t)] \right\rangle \tag{8}$$

where G_s and G_d are called the *self*- and *distinct*-part because G_s correlates positions of the same particle ($j = l$) at different times while G_d correlates positions of different particles ($j \neq l$). $G_s(\mathbf{r}, t)$ gives the probability that within time t a particle moves by $\mathbf{r}$, while $G_d(r, t)$ gives the probability of finding any different particle at distance $\mathbf{r}$ from the former position of some particle. Hence, for a homogeneous system (fluid), the self-part turns out to be just the propagator of the probability.

By eq 2, Fourier transform with respect to the space of the van Hove correlation function yields the intermediate scattering function, whereas by eq 1, transform with respect to both time and space yields the dynamic structure factor. Because of the linearity of the Fourier transform, the same relationship holds for self- and distinct-parts, separately. Here we restrict ourselves to the self-part.

G_s, F_s, and S_s in the Hydrodynamic Limit. In statics, for distances of only some molecule diameters, a liquid can already be treated as a continuum. As for dynamics, the time scale needs to be taken into account, too.[7] Suppose that for the system under consideration the diffusion equation holds, at least on the hydrodynamic scale, i. e., there exist some characteristic length l and time τ such that for $l \ll x$ and $\tau \ll t$

$$\frac{\partial \bar{\rho}(\mathbf{r}, t)}{\partial t} = D_s \nabla^2 \bar{\rho}(\mathbf{r}, t) \tag{9}$$

In Fourier space this reads

$$\frac{\partial \bar{\rho}_{\mathbf{k}}(t)}{\partial t} = -D_s k^2 \bar{\rho}_{\mathbf{k}}(t) \tag{10}$$

which is easily integrated to give

$$\bar{\rho}_{\mathbf{k}}(t) = \bar{\rho}_{\mathbf{k}}(0) \exp\{-D_s k^2 t\} \tag{11}$$

The bar indicates a hydrodynamic observable obtained from its microscopic equivalent by coarse-graining. The normalized autocorrelation function is

$$\frac{1}{N}\langle \bar{\rho}_{\mathbf{k}}(t) \bar{\rho}_{-\mathbf{k}}(0) \rangle = \exp\{-D_s k^2 t\} \tag{12}$$

Following Onsager[8] we can, in the hydrodynamic limit, identify this correlation with the corresponding microscopic correlation function, given by eq 2. Moreover, for a dilute species, one obtains[7] in the limit $kl \ll 1$ and $\tau/t \ll 1$

$$F_s^{hyd}(k, t) = \exp\{-D_s k^2 t\} \tag{13}$$

$$G_s^{hyd}(r, t) = \frac{1}{(4\pi D_s t)^{3/2}} \exp\{-r^2/4D_s t\} \tag{14}$$

$$S_s^{hyd}(k, \omega) = \frac{1}{\pi} \frac{D_s k^2}{\omega^2 + (D_s k^2)^2} \tag{15}$$

In other words, we have exponential decay for long times of the Fourier components with long wavelengths, a Gaussian curve for G_s^{hyd}, and a Lorentzian curve of half width at half maximum $\Omega = D_s k^2$ at $\omega = 0$ for S_s^{hyd}. The exponential decay for long times of the Fourier components with long wavelengths, eq 13, allows for determination of the self-diffusivity:

$$D_s = -\frac{1}{k^2 t} \ln F_s^{hyd}(k, t) \tag{16}$$

Using eq 10, we have presumed isotropy for convenience, but all considerations in this text can be extended to the anisotropic case as well.

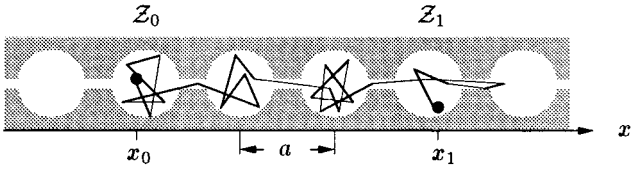

Figure 1. A simple model for the zeolite ZK4.

Diffusion of Guest Molecules in a Crystal. As the crystal is not homogeneous on a microscopic length scale, any correlation in space will depend on *both* positions, not only on their difference. Hence, we must restore the homogenizing integral in eq 4. Without loss of generality we restrict ourselves to one-dimensional diffusion along the x-axis. Denoting by $P(x_1, t; x_0)$ the probability density that some arbitrarily chosen particle is at point x_1 at time t *and* was at point x_0 initially, we have from eq 7

$$\begin{aligned} G_s(x, t) &= \int_0^a P(x_0 + x, t; x_0)\, dx_0 \\ &= \int_0^a p(x_0 + x, t|x_0) P(x_0)\, dx_0 \end{aligned} \tag{17}$$

where a is the lattice constant, $p(x_1, t|x_0)$ is the density of the conditional probability of finding the particle at position x_1 at time t *if* it was at x_0 at the beginning, and $P(x)$ is the (stationary) probability density of finding a given particle near point x. Because it is periodic in space, the normalization is chosen to be $\int_0^a P(x)dx = 1$. The second line is simply a well-known identity from the theory of probabilities.

On a length scale coarse compared with a, however, the crystal can be regarded again as a continuum. Thus, applying eq 14 to the one-dimensional case,

$$G_s(x, t) \rightarrow G_s^{hyd}(x, t) = \frac{1}{\sqrt{4\pi D_s t}} \exp\left[-\frac{x^2}{4D_s t}\right] \tag{18}$$

On a finer length scale the self-part of the van Hove function for the diffusion in a crystal is approximately equal to this hydrodynamic limit $G_s^{hyd}(x, t)$, modulated by a function $I(x)$ with lattice periodicity:

$$G_s(x, t) \approx G_s^{hyd}(x, t) I(x) \tag{19}$$

An Approximation Formula for $I(x)$. Under special conditions, the motion of a guest molecule in a porous crystal can be separated into partial motions, each having a time scale of its own. Methane molecules in an A-type zeolite, for example, preferably reside in large cavities of radius R and seldom switch from one cavity to the other. This situation is sketched for one direction in Figure 1.

Equation 17 is exact, but as the transition probability $p(x_1, t|x_0)$ is unknown, one would like to approximate it by quantities which are available. According to eq 17, only

transitions with both starting and final points lying within a permitted region contribute to G_s. Hence, x_0 and x_1 can be assumed to be within cells Z_0 and Z_1.

Now we introduce the following notations: $p(x_j, t_j|Z_i, t_i)$ is the probability density of finding the particle at position x_j at time t_j provided that it was in cell Z_i at time t_i, with normalization $\int_{-\infty}^{\infty} p(x_j, t_j|Z_i, t_i)dx_j = 1$. For the probability of finding it in cell Z_j at time t_j given that it was in Z_i at time t_i, we write $p(Z_i, t_j|Z_i, t_i)$. The probability of finding the particle in cell Z_j at time t_j if it was at point x_i at time t_i is $p(Z_j, t_j|x_i, t_i)$. Note that Z is a discrete quantity, whereas x is continuous. Hence, $p(x_j, t_j|Z_i, t_i)$ and $P(x)$ are probability *densities*, while $p(Z_j, t_j|Z_i, t_i)$ and $p(Z_j, t_j|x_i, t_i)$ are probabilities. Furthermore, as we are dealing with a stationary system, all transition probabilities depend on the time *differences* only.

By the Markovian character of the motion we have

$$p(x_1, t|x_0, 0) = p(x_l, t|Z_1, t)\, p(Z_1, t|Z_0, 0)\, p(Z_0, 0|x_0, 0) \tag{20}$$

Because being at position x_j implies being within Z_j at the same time, by definition,

$$p(Z_j, t|x_j, t) = 1 \tag{21}$$

for all t, i. e., the last factor in eq 20 is simply 1. Now the probability density $p(x_j, t|Z_j, t)$ for finding the particle at x_j at time t, given that it is in the right cell, is equal to the equilibrium spatial probability density $P(x_j)$, independent of time,

$$p(x_1, t|Z_1, t) = P(x_1) \tag{22}$$

This is because the time intervening between intercell jumps is very long compared to the time required for the particle to move through a cell. By virtue of this time scale separation, for the times of interest here, we can assume that the particle thermalizes (assumes its equilibrium distribution) in a cell instantaneously, as soon as it enters the cell.

Evidently the hopping rate for an intercell jump depends only upon the number of cells in between Z_0 and Z_1, n. For $a > 4R$, the number of intercells is a unique step function of.the distance $|x_1 - x_0|$, otherwise it varies by 1 depending on x_0. However, for large distances this becomes unimportant, and so does the difference between the exact distance of the cells, na, and $|x_1 - x_0|$. We therefore let

$$p(Z_1, t|Z_0, 0) \approx aG_s^{hyd}(x_1 - x_0, t) \tag{23}$$

where again the factor a follows from normalization, $\int_{-\infty}^{\infty} G_s^{hyd}(x, t)dx = 1$ and $1 = \sum_j p(Z_j, t|Z_0) \approx \int_{-\infty}^{\infty} a^{-1}p(Z_j, t|Z_0)dx_j$.

Approximation (23) along with eqs 22 and 21 yields

$$p(x_i, t|x_0) \approx aP(x_1)\, G_s^{hyd}(x_1 - x_0, t) \tag{24}$$

Inserting this into eq 17 and factoring $G_s^{hyd}(x, t)$ out of the integral, one obtains

$$G_s(x, t) \approx G_s^{hyd}(x, t)I(x) \tag{25}$$

where $I(x)$ is the space autocorrelation function of the probability $P(x)$,

$$I(x) = a\int_0^a P(x_0 + x)P(x_0)\, dx_0 \tag{26}$$

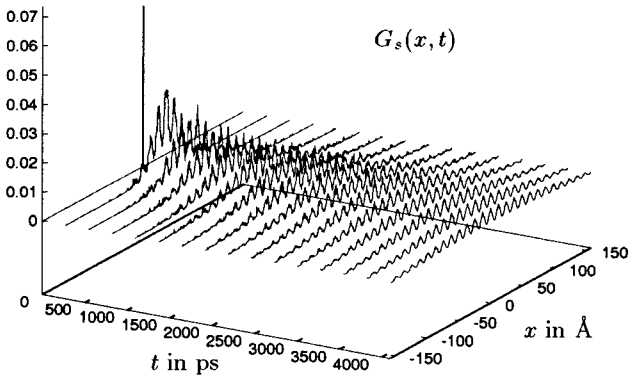

Figure 2. Self-part $G_s(x, t)$ of the van Hove correlation function for the diffusion of methane in ZK4 at $n_{occ} = 3$ and $T = 300$ K.

The result eq 25 can be interpreted as follows: The van Hove function for the diffusion in a periodic structure is the Gaussian describing diffusion in a homogeneous medium of the same diffusivity, but modulated by some structure function. This function can be approximated by the space autocorrelation function of the probability density of the diffusants.

The Radial van Hove Function. Since $G_s(\mathbf{r}, t)$ is the density of the probability that a particle moves within t by $\mathbf{r}$ (in a particular direction), the solid angle integral

$$g_s(r, t) \doteq \int_{\vartheta=0}^{\pi}\int_{\varphi=0}^{2\pi} G_s(\mathbf{r}, t)\, r^2 \sin\vartheta\, d\varphi\, d\vartheta \tag{27}$$

yields the probability density that it moves by the distance r, regardless of the direction. In case of isotropy, $G_s(\mathbf{r}, t) = G_s(r, t)$, resulting in $g_s(r, t) = 4\pi r^2\, G_s(r, t)$. Consequently it makes sense to *define* the radial van Hove function in the anisotropic case by

$$G_s(r, t) \doteq \frac{1}{4\pi r^2} g_s(r, t) \tag{28}$$

No matter whether $G_s(r, t)$ denotes this orientational average of $G_s(\mathbf{r}, t)$ or is identical to $G_s(\mathbf{r}, t)$ due to isotropy, the intermediate scattering function and the dynamic structure factor defined using $G_s(r, t)$ in eq 2 and 1 are isotropic and are denoted by $F_s(k, t)$ and $S_s(k, \omega)$. In the hydrodynamic limit, $G_s(r, t)$, $F_s(k, t)$, and $S_s(k, \omega)$ are given by eq 14, 13, and 15, respectively. The radial van Hove function makes a comparison with results from neutron scattering experiments possible.

Results from MD Simulation

Van Hove Function (self-part) for ZK4. We start with ZK4 at room temperature ($T = 300$ K) and an average loading of three CH_4 molecules per unit cell, $n_{occ} = 3$. The self-part of the van Hove correlation function, $G_s(x, t)$, is shown in Figure 2. Sections are drawn every 273 ps starting at $t = 0$ and ending with $t = 4095$ ps. The singular δ-peak at $t = 0$ has been cut. One recognizes the shape of this function of two variables, mentioned above: an at least approximately Gaussian curve broadening and fading away as time goes on, modulated with the lattice periodicity. Notice that the area in the tx-plane where the function is noticeably larger than zero has a parabolic border as is to be expected, because $\langle x^2\rangle \sim t$.

As loading increases the diffusivity is reduced, resulting in a narrower bell-shaped curve. The effect is hardly observable at low loadings but it becomes quickly important above $n_{occ} = 6$, and at $n_{occ} = 15$ the molecules are almost fixed. This is in agreement with results from MSD.[9,10]

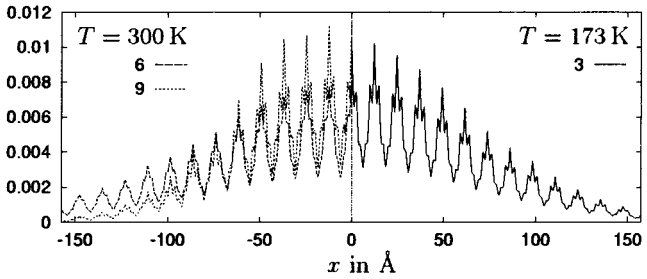

Figure 3. The section through $G_s(x, t)$ at $t = 4095$ ps for $n_{occ} = 3$ at 173 K lies between the curves for $n_{occ} = 6$ and $n_{occ} = 9$ at 300 K, but its structuring is more pronounced.

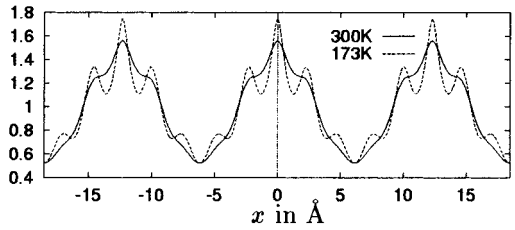

Figure 4. The correlation function $I(x)$ of the probability density $P(x)$ for $n_{occ} = 3$ at $T = 173$ K and $T = 300$ K. At lower temperature the molecules are located at their favorite sites, so the fine structuring is more pronounced.

Reducing the temperature has a similar effect. As can be seen from Figure 3, the curve for $n_{occ} = 3$, $T = 173$ K lies between those for $n_{occ} = 6$ and $n_{occ} = 9$ at $T = 300$ K. This implies that the diffusion coefficient at 173 K and three molecules per unit cell must have some value between the corresponding D_s at 300 K, which is also in accordance with MSD results. Looking more carefully, one finds that the "shoulders" of the right curve are more pronounced. This is reasonable as a lower temperature not only impedes a particle's progress (diffusion) but also reduces its local thermal motion which smears the fine structure.

The Approximation by $G_s^{hyd}(x, t)I(x)$. We now wish to test the approximation formula eq 25 derived above. As already mentioned, the approximation should be good except for very short times and distances. The space autocorrelation function, $I(x)$, of the probability density $P(x)$ is shown in Figure 4 for an interval of three elementary cells. Clearly the curve is less smooth at lower temperature. Its shape follows immediately from that of $P(x)$, which again can be understood easily by looking at the three-dimensional density.[9] As maxima of $P(x)$ stand for specific sites prefered by the methane molecules, maxima of $I(x)$ represent transitions between such sites.

In Figure 5 the approximation is compared with the function $G_s(x, t)$ from the simulation. The agreement is excellent. At low loading and higher temperature, both curves are practically congruent (top). For mean loadings, some discrepancies appear, particularly at small distances (middle). The comparison is of greatest interest at low temperature (bottom) because the fine structure is most pronounced there. The only major difference is that for $G_s(x, t)$ the "shoulders" seen in the fine structure are symmetric with respect to the maximum in between, while in the approximation the one closer to the overall maximum of the Gauss curve is naturally larger. This is caused by the approximation in eq 23: Strictly speaking, as long as the final destination is within one and the same cell, the transition probability depends on the local density, not on the distance. Consequently, the Gaussian would have to be replaced by a step function with stairs symmetric with respect to the centers

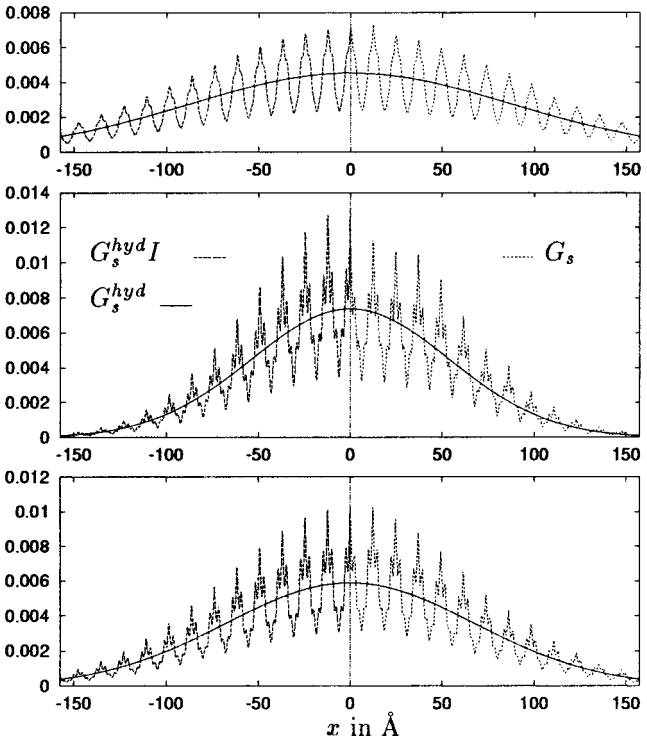

Figure 5. Comparison of $G_s(x, t)$ with the approximation $G_s^{hyd}(x, t)$-$I(x)$ at $t = 4095$ ps. Top: $n_{occ} = 3$, $T = 300$ K. Middle: $n_{occ} = 9$, $T = 300$ K. Bottom: $n_{occ} = 3$, $T = 173$ K. The approximation is shown on the left, the exact van Hove function on the right-hand side, and the Gaussian $G_s^{hyd}(x, t)$ on both sides of the plots.

of the cells to get perfect agreement between the exact G_s and the approximation.

Van Hove Function (Self-Part) for Silicalite. In the three graphs of Figure 6 the self-part of the van Hove function in silicalite is shown along the *x*-, *y*-, and *z*-directions. Parameters ($T = 300$ K, $n_{occ} = 3$) and representation (one intersection every 273 ps) are the same as in the equivalent picture for ZK4, Figure 2. In comparison, fluctuations have increased. The parabolic propagation in time−distance coordinates can be seen here as well. Obviously, the curve for the *y*-direction fades away a bit faster, and the curve for the *z*-direction much more slowly than the one for the *x*-direction. The *tz* parabola is so narrow, that wide strips occur on either side where the function is zero (and therefore is not drawn). All of these facts are in accord with both intuition (highest mobility along the straight *y*-channels, still high mobility along the zig-zag channels in the *x*-direction, substantially lower mobility in the *z*-direction where the particle has to make detours) and results from mean-square displacement. The dependency of G_s on n_{occ} and T is the same as for ZK4, qualitatively, except that silicalite can adsorb much more methane molecules per unit cell.

It is interesting to examine how the approximation eq 25 which was inspired by the ZK4 structure can be justified for silicalite. The space correlation functions $I(x)$, $I(y)$, and $I(z)$ of the one-dimensional probability densities for the *x*-, y-, and *z*-directions are depicted in Figure 7. For the sake of brevity, these functions are shown over a domain equal in length to the respective lattice constant. One must not get deceived by the periodicity: The one-dimensional densities are periodic within half-lattice constants, for symmetry reasons (screw axes), and their space correlation functions inherit this property. As in the case of ZK4, the shape of the space correlations can be interpreted quite well by considering the three-dimensional density, particularly the sites of maximum density.[9,11,12]

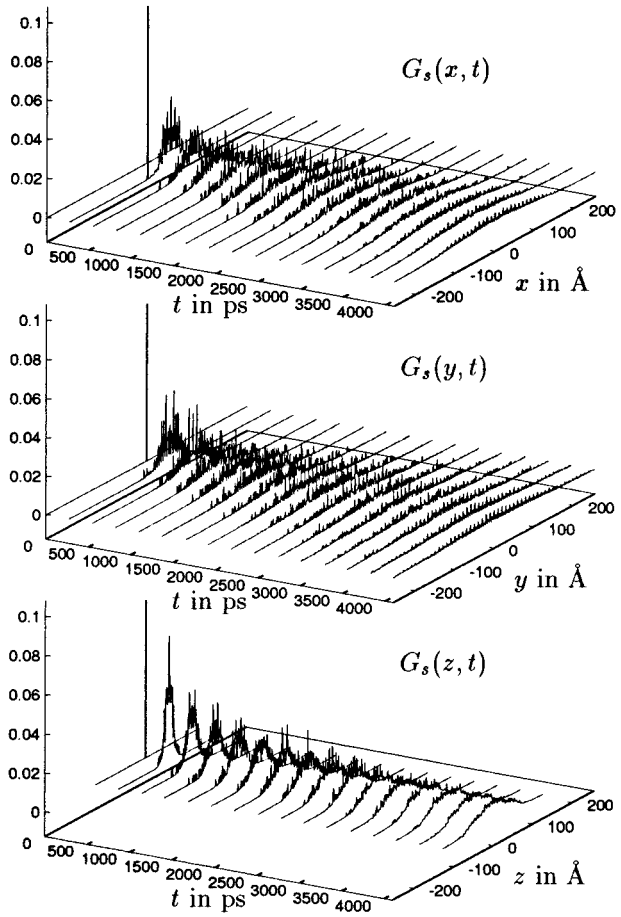

Figure 6. Self-part G_s of the van Hove correlation function for the diffusion of methane in silicalite in *x*-, *y*-, and *z*-directions at $n_{occ} = 3$ and $T = 300$ K.

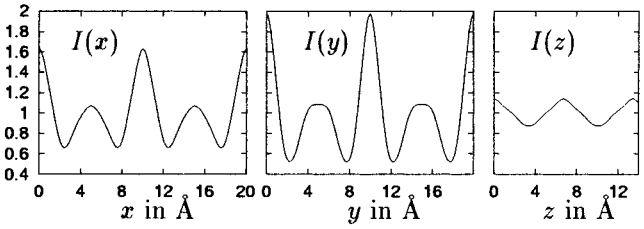

Figure 7. The correlation functions $I(x)$, $I(y)$, and $I(z)$ for silicalite at $n_{occ} = 3$ and $T = 300$ K. Note the periodicity with characteristic length equal to one half of the lattice constants.

On the basis of the simulation data, the detailed shape of the van Hove correlation function cannot be resolved. So we choose a different way of representation for the comparison with the approximation. Unlike for ZK4 (cf. Figure 5), the original function and its approximation are plotted on top of each other in Figure 8. The points for G_s lie on the approximating curve for the most part. In the *y*-direction, discrepancies occur only for very small *y*. In the *x*- and *z*-directions, differences are also obtained for larger distances (around 100 or 50Å, respectively), but the approximation improves as distance grows. This confirms that formula 25 is not restricted to ZK4 but holds more generally for systems where a rapid motion of particles within restricted regions adds to a slow motion between such regions.

The Intermediate Scattering Function for ZK4. Figure 9 shows the self-part $F_s(k, t)$ of the scattering function obtained by Fourier transform of the function $G_s(x, t)$ shown in Figure 2. At the beginning we have a white spectrum, i.e., $F_s(k, 0) = const$, which is the transform of the initial δ-peak $G_s(x, 0)$. Most

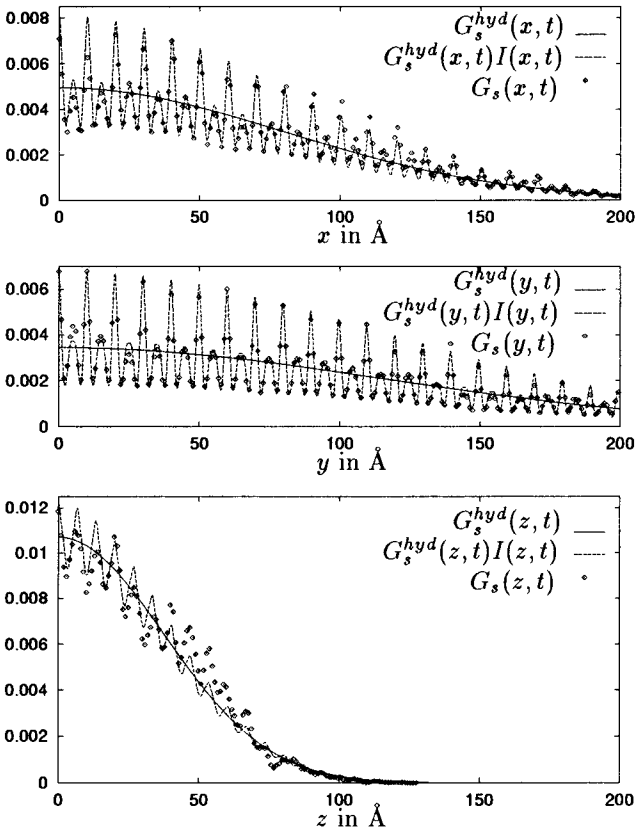

Figure 8. Comparison of G_s with the approximation $G_s^{hyd}I$ in silicalite at $t = 4095$ ps for $n_{occ} = 3$, $T = 300$ K. From top to bottom: *x*-, *y*-, and *z*-direction.

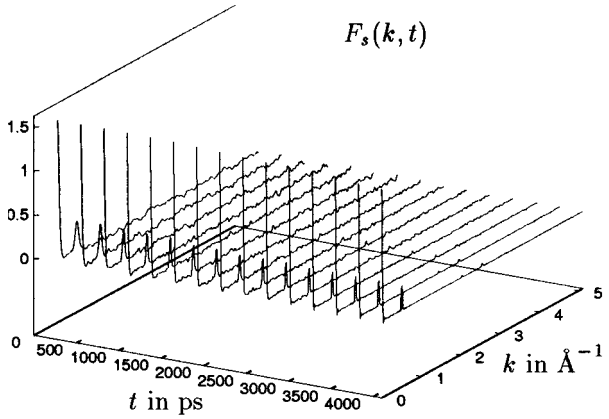

Figure 9. Self-part $F_s(k, t)$ of the scattering function for methane in ZK4 at $n_{occ} = 3$ and $T = 300$ K.

of the spectral components decay quickly, the shorter the wavelength the faster the decay. Few lines remain, for instance the line at zero, and so arises a discrete spectrum.

The major lines can be interpreted very easily. To this end we look at the spectrum at a lower temperature, where the fine structure is sharper, Figure 10. By far the strongest line is the one at $k = 0$: the Fourier transform of the Gaussian hydrodynamic limit. Next follows the line around 0.5 Å^{-1}, which is just 2π times the reciprocal lattice constant of ZK4 ($a = 12.3$ Å). Consequently, this line represents the periodic modulation. Also the line near 2.55 Å^{-1} can be interpreted. It originates in the side maxima (or shoulders) of $G_s(x, t)$ because of the detailed distribution of the molecules to specific sites. That's why it almost vanishes at 300 K where the shoulders are very weak, cf. Figures 4 and 5, indicating a rather smooth distribution within

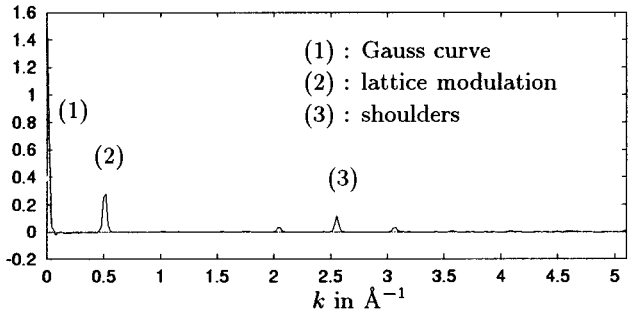

Figure 10. Intersection through $F_s(k, t)$ at $t = 4095$ ps. ZK4, $T = 173$ K.

TABLE 1: Range of Values of *x*, *t*, *k*, and ω for which G_s, F_s, and S_s were determined

	ΔQ		Q_{max}	
quantity Q	ZK4	silicalite	ZK4	silicalite
x in Å	0.615	0.996	315[a]	510[b]
k in 10^{-2} Å^{-1}	1.995[a]	1.232[b]	511	315
t in ps	1.0		4095	
ω in ps^{-1}	7.67×10^{-4}[c]		3.142	

[a] For $n_{occ} = 15$, x_{max} is half, Δk twice this value. [b] For *z*-direction, z_{max} is half, Δk_z twice this value. [c] Using symmetry $F(k, -t) = F(k, t)$.

the cells. As $G_s(x, t)$ is a periodic function (except for the slow Gaussian damping), its spectrum should contain components only at multiples of $2\pi/a$ (except for small wave numbers). This is confirmed.

From eq 13, the long-wave components of $F_s(k, t)$, i.e., those with small k, are expected to decay in time exponentially,

$$F_s(k, t) \sim \exp\{-D_s k^2 t\} \tag{29}$$

First, the region of validity of this approximation has to be determined. The part of the hydrodynamic limit in eq 13 regarding space has to be related to a and means $k \ll 2\pi a^{-1} \sim 0.8$ Å^{-1}. For a lower bound of time we use the so-called Einstein relation

$$\langle |\mathbf{r}(t) - \mathbf{r}(t_0)|^2 \rangle = 6D(t - t_0) \tag{30}$$

to find $t \geq a^2/2D_s$. For $D_s \approx 10^{-8}$ m^2/s this finally yields $t \geq 72$ ps. As our data start only at 100 ps, we are not further restricted in time, at least for loadings up to $n_{occ} = 9$.

Experimental or simulation data are always discrete and bounded. Because of the reciprocal character of the Fourier transform, this limits the resolution of k and ω. The minimum and maximum lengths and times registered, Δx, x_{max} and Δt, t_{max}, respectively, and the corresponding maximum and minimum wave numbers and frequencies, k_{max}, Δk and ω_{max}, $\Delta\omega$, are listed in Table 1, both for ZK4 and silicalite.

The first three components available of the intermediate scattering function, i.e., $F_s(k, t)$ at k = 0, $k = \Delta k$, and $k = 2\Delta k$, are depicted in logarithmic scale in Figure 11. All curves start at the same initial value. The zero components are constant in time. The second line ($k = \Delta k$) is a falling straight line for all loadings while the third one deviates soon for low loadings ($n_{occ} = 9$ and even more $n_{occ} = 3$). Furthermore, the third line has four times the slope of the second. This is true even in the upper pictures as long as the third line is straight. Thus the slope grows quadratically with k, as predicted by eq 29. Resolving for the diffusion coefficient yields

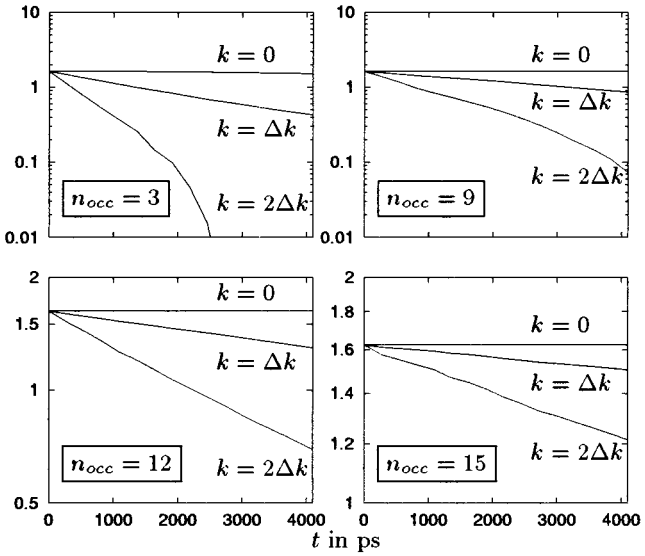

Figure 11. Decay of the first three components of $F_s(k, t)$ for different n_{occ} in ZK4 in logarithmic scale. Note the different scales of the vertical axes.

$$D_s = \frac{\ln F_s(k, 0) - \ln F_s(k, t)}{k^2 t} \tag{31}$$

The values for D_s obtained this way from the exponential decay of $F_s(k, t)$ are summarized in Table 2 along with those from MSD (in brackets). The agreement is good. As the motion over short length scales is not quite diffusive, deviations from this linearity occur at larger k.

The Intermediate Scattering Function for Silicalite. Because the development in time of the intermediate scattering function is the same for silicalite as for ZK4, we just glance at the sections through F_s for $t = 4095$ ps, Figure 12. What has been said about periodicity remains valid, except that we are dealing now with half-lattice constants in silicalite, i.e., $a/2$, $b/2$, and $c/2$. This is a consequence of the symmetry of the crystal, more precisely of its screw axis.[9] Again the zero k line is the largest contribution to the spectra. Next come the lines at $k = 4\pi/a$, $4\pi/b$, or $4\pi/c$, respectively, representing the modulation by the lattice. For the *z*-direction, there is no other component of significance, the curve $I(z)$ in Figure 7 has indeed almost cosinusoidal shape. In contrast, the side maxima of $I(x)$ and $I(y)$ lead to an additional line at $k = 8\pi/a$ and $8\pi/b$.

As was done in Figure 11 for ZK4, the first three components of the spectrum for silicalite are depicted in Figure 13 for the *x*-, *y*-, and *z*-directions and for $n_{occ} = 3$ (top) and $n_{occ} = 12$ (bottom). Again, deviations occur in the third component at low loading. The values for the self-diffusivity determined from the decay with eq 31 are listed in Table 3. Satisfactory agreement with those obtained from MSD (in brackets) is observed.

The Dynamic Structure Factor for ZK4. The self-part of the dynamic structure factor in ZK4 is shown in Figure 14 for $n_{occ} = 3$ and $T = 300$ K. Only a small part of the possible area is depicted, because $S_s(k, \omega)$ is negligible outside. Recall that this function is the Fourier transform with respect to time of the intermediate scattering function in Figure 9. Hence, we find the line spectrum for long times from Figure 10 at $\omega = 0$. All components vanish for higher frequencies, those having wave numbers smaller than ca. 0.1 Å^{-1} first.

According to eq 15, $S_s(k, \omega)$, as a function of ω at fixed k, becomes a Lorentz curve of half width at half maximum

TABLE 2: D_s in ZK4 from the Decay of the Long-Wavelength Components of the Scattering Function and from MSD, in Parentheses[a]

	D_s (in 10^{-9} m^2/s)			
n_{occ}	from Δk	$2\Delta k$	$3\Delta k$	MSD
3	8.17			(9.46)
6	7.14			(7.19)
9	3.87	4.75		(3.56)
12	1.39	1.30	1.20	(1.42)
15	0.12	0.11	0.10	(0.12)

[a] For Δk see Table 1.

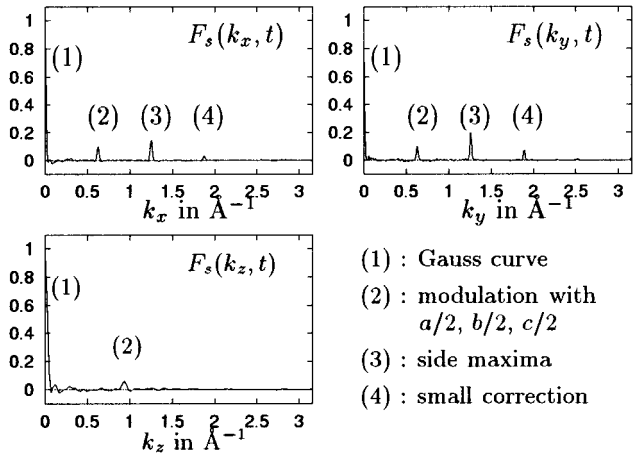

Figure 12. Intersections through F_s at $t = 4095$ ps for silicalite, the spectra of the curves shown in Figure 8. The most important lines can be interpreted very easily, noticing that the modulation is with half the lattice periods.

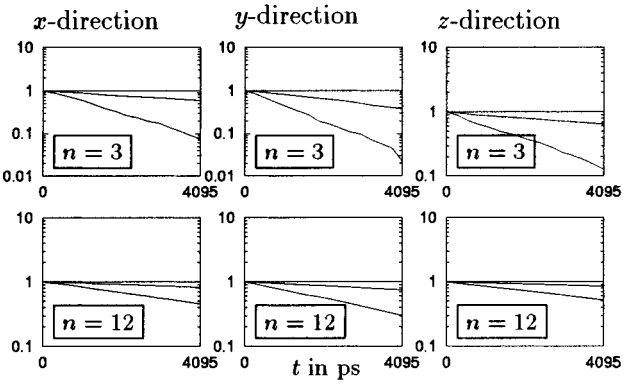

Figure 13. The first three components of $F_s(k, t)$ with $k = 0$, $k = \Delta k$, and $k = 2\Delta k$ for the three principal directions in silicalite at $n_{occ} = 3$ and 12 in logarithmic representation.

$$\Omega = D_s k^2 \tag{32}$$

in the hydrodynamic limit. In our attempt to prove this rule for the diffusion of methane in ZK4 or silicalite we are limited by the resolution. For the shape of the curve to be visible, the smallest frequency interval resolved must be below the half width, i.e.,

$$\Delta\omega \ll D_s k^2 \tag{33}$$

Now, in ZK4, D_s is merely about 10^{-8} m^2/s even at low loadings, which together with $\Delta\omega$ from Table 1, means $k \gg 2.8 \times 10^{-2}$ Å^{-1}. But from the decay of the intermediate scattering function we have seen that the long-wave regime reaches only out to a few Δk, not even to 0.1 Å^{-1}. So the exact shape of the curve becomes visible only near the border of the region where eq 15 is valid. In Figure 15, the points of the first three lines with $k > 0$ are depicted along with the ideal Lorentzian curves for $D_s = 9.5 \times 10^{-9}$ m^2/s from MSD. Agreement is excellent, particularly for the second curve which seems to offer the best compromise between the upper bound (the hydrodynamic limit) and the lower bound (resolution).

TABLE 3: D_s^x, D_s^y, and D_s^z in Silicalite from the Decay of the Long-wavelength Components of the Scattering Function and from MSD, in Parentheses[a]

n_{occ}	k	D_s^x in 10^{-9} m^2/s	D_s^y in 10^{-9} m^2/s	D_s^z in 10^{-9} m^2/s
3	Δk	8.51 (7.89)	15.60 (16.35)	1.78 (1.70)
6	Δk	5.94 (6.09)	8.53 (8.65)	1.38 (1.37)
	$2\Delta k$	5.42	7.85	1.48
9	Δk	4.72 (4.69)	6.42 (5.65)	0.92 (0.99)
	$2\Delta k$	4.47	6.36	0.91
12	Δk	3.26 (3.08)	4.74 (4.52)	0.66 (0.68)
	$2\Delta k$	3.17	4.86	0.66
15	Δk	1.63 (1.66)	4.03 (4.17)	0.43 (0.49)
	$2\Delta k$	1.63	3.98	0.42

[a] For Δk and t_{max} see Table 1.

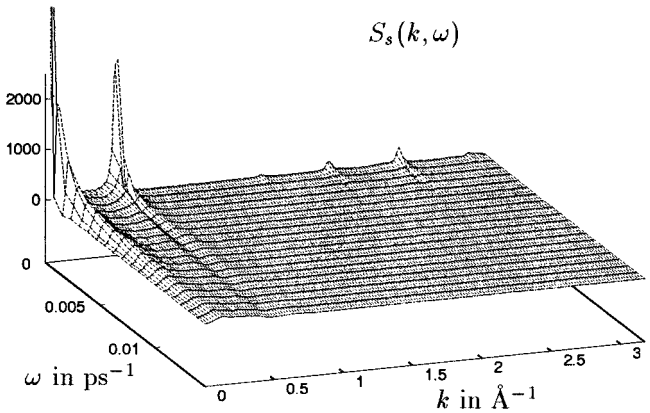

Figure 14. Self-part $S_s(k, \omega)$ of the dynamic structure factor for methane in ZK4 at $n_{occ} = 3$ and $T = 300$ K.

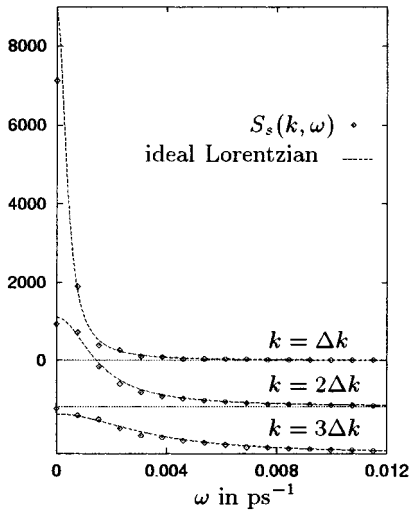

Figure 15. The Lorentz curve predicted for $S_s(k, \omega)$ (at fixed k) in the hydrodynamic limit (broken line) and the result from MD (points) for $k = \Delta k$, $2\Delta k$, and $3\Delta k$ in ZK4.

The Dynamic Structure Factor for Silicalite. The three pictures in Figure 16 show the self-parts of the dynamic structure factors for the *x*-, *y*-, and *z*-direction, $S_s(k, \omega)$, $S_s(k_y, \omega)$, and $S_s(k_z, \omega)$. As for ZK4, we have the same line spectrum at small frequencies as results in the limit of long times for $F_s(k_x, t)$,

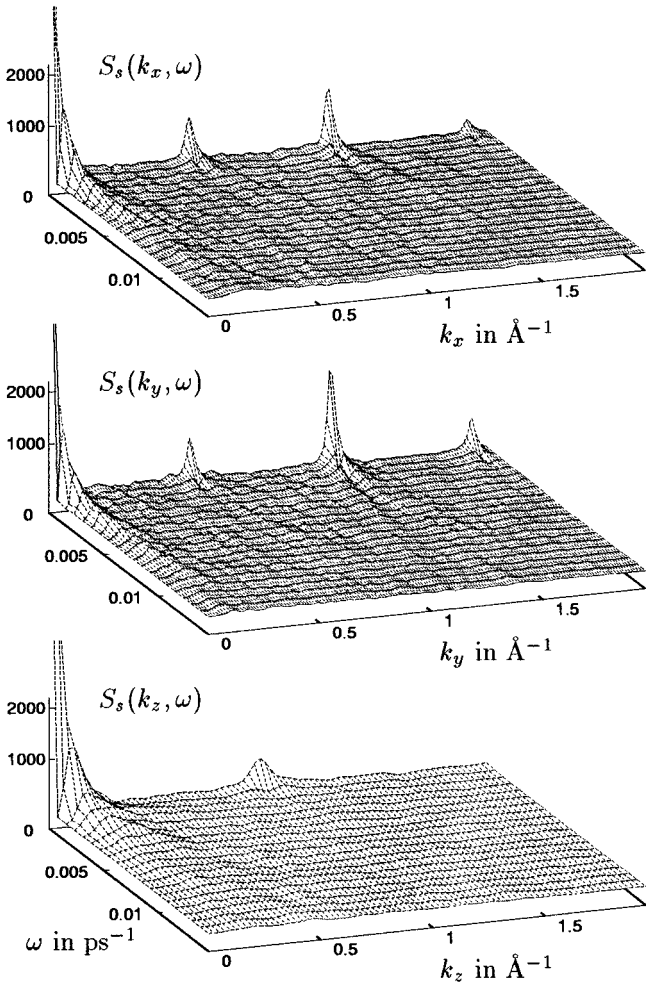

Figure 16. Self-part S_s of the structure factor in *x*-, *y*-, and *z*-directions for methane in silicalite at $n_{occ} = 3$ and $T = 300$ K. For the resolution in k_z see Table 1.

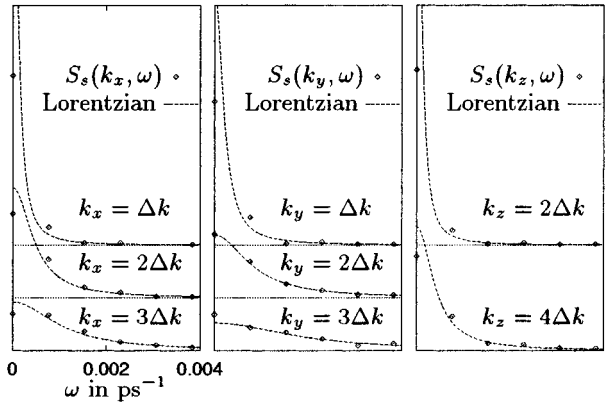

Figure 17. The Lorentz curves predicted for S_s (at fixed k) in the hydrodynamic limit (broken lines) and the results from MD (points) for Δk, $2\Delta k$, and $3\Delta k$ (*x*- and *y*-direction) or $2\Delta k$, $4\Delta k$ (*z*-direction). Silicalite, $\Delta k = 1.23 \times 10^{-2}$ Å^{-1}.

$F_s(k_y, t)$, and $F_s(k_z, t)$, cf. Figure 12. For higher frequencies the components vanish quickly.

In Figure 17, the computed small k S_s is compared to the Lorentzian predicted by eq 15 in the hydrodynamic limit. Because of the slow propagation in the *z*-direction the resolution we could use in this direction is only half as fine. Therefore, in Figure 17 the components with $2\Delta k$ and $4\Delta k$ are shown for $S_s(k_z, \omega)$ instead of those with Δk, $2\Delta k$, and $3\Delta k$. For

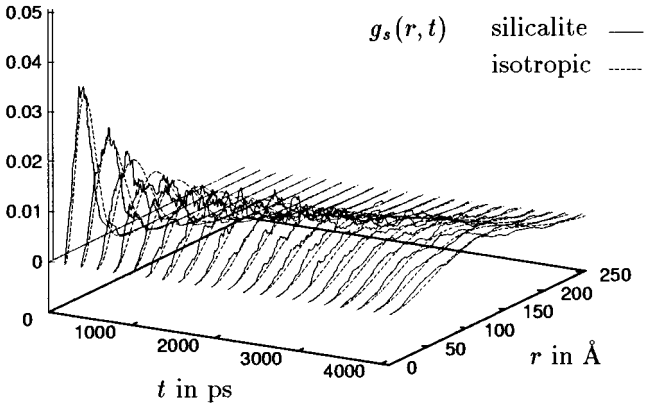

Figure 18. $g_s(r, t)$ according to eq 27 for methane in silicalite at $n_{occ} = 3$, $T = 300$ K, compared with the isotropic case (broken lines).

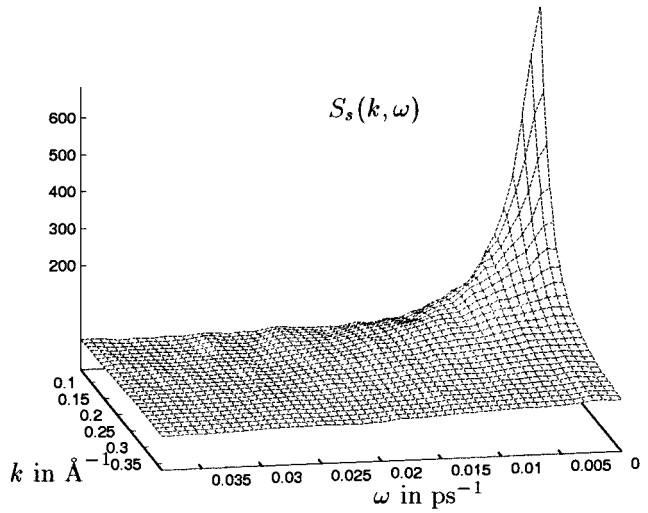

Figure 19. Self-part of the radial dynamic structure factor $S_s(k, \omega)$ in silicalite at $n_{occ} = 3$ and $T = 300$ K.

constructing the Lorentz curves the, self-diffusion coefficients from MSD were used, $D_s^x = 8 \times 10^{-9}$ m^2/s, $D_s^y = 14 \times 10^{-9}$ m^2/s, and $D_s^z = 1.7 \times 10^{-9}$ m^2/s. The agreement is not as good as in the case of ZK4, but still acceptable.

The Radial van Hove Function for Silicalite. Obviously, the self-part of the radial van Hove function, $G_s(r, t)$, starts with $G_s(r, 0) = \delta(r)$ and then decays in the same way as $G_s(\mathbf{r}, t)$, the maximum always remaining at $r = 0$. The maximum of $g_s(r, t)$, in contrast, moves towards larger radii because of the weighting with $4\pi r^2$. In the hydrodynamic limit, the dependence of the distances at which these maxima occur on time is described by the parabola $r^2 = 4D_s t$. Figure 18 shows $g_s(r, t)$ for methane in silicalite along with the solid angle integral of the ideal Gaussian from eq 14, calculated with $D_s = 8.6 \times 10^{-9}$ m^2/s from the mean square displacement. No major differences are observed.

As the radial van Hove function $G_s(r, t)$, unlike $G_s(\mathbf{r}, t)$, averages. over different directions, it does not reveal the periodicity and symmetry of the crystal and it soon loses any fine structure. This implies that no line spectrum is to be expected for the radial intermediate scattering function $F_s(k, t)$ for long times. The same is true for the dynamic structure factor at low frequencies. This is confirmed in Figure 19: The curve $S_s(k, 0)$ (right border) decays smoothly. As the range of k is from $k = 5\Delta k$ to $30\Delta k$ (which means 0.061 to 0.370 Å^{-1}), the hydrodynamic limit is valid in the backmost part of the graph and the shape of $S_s(k, \omega)$ ought to be Lorentzian with half width at half maximum $\Omega = D_s k^2$. One can see that the width grows

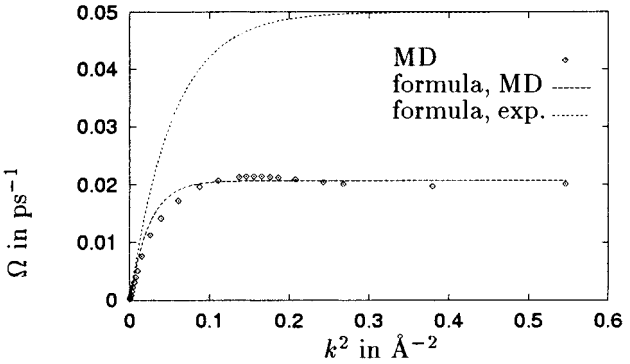

Figure 20. The half width at half maximum Ω of $S_s(k, \omega)$ as function of k^2 together with the curve fitted according to eq 34. The corresponding curve based on extrapolated experimental data, cf. ref 14.

TABLE 4: Experimental Results from Ref 14 and Their Extrapolation to Our Conditions[a]

$T = 200$ K			$T = 250$ K			$T = 300$ K	
n_{occ}	τ (ps)	$D_s \times 10^9$ (m²/s)	n_{occ}	τ (ps)	$D_s \times 10^9$ (m²/s)	τ (ps)	$D_s \times 10^9$ (m²/s)
2	65	2.8	1.5	36	5.0		
4	50	2.5	2.8	30	5.9		
3	57	2.7	3	29	6.0	20	9.3

[a] The values extracted from our simulation analyis at 3 molecules per unit cell and 300 K are $\tau = 48$ ps and $D_s = 8.6 \times 10^{-9}$ m²/s.

in fact up to the middle region of k studied but stagnates thereafter. The shape of the curve remains Lorentzian, even for the frontmost curves which are far from the hydrodynamic limit.

According to ref 13 a jump model, where the width of a jump follows a normal distribution and the rate of jumps follows a Poisson distribution with mean τ^{-1}, leads to a Lorentzian dynamic structure factor of half width at half maximum

$$\Omega = \frac{1}{\tau}(1 - \exp\{-D_s k^2 \tau\}) \qquad (34)$$

For small k, one recovers $\Omega = D_s k^2$, whereas for $k \rightarrow \infty$ the value $1/\tau$ is reached asymptotically. Widths obtained from quasielastic neutron scattering obey this law quite well.[14] The course of our computed $S_s(k, \omega)$ curve just discussed exhibits a similar behavior. Figure 20 shows the dependence on the square of the wave number of the half widths of Lorentzian fits to $S_s(k, \omega)$. A fit based on eq 34 is drawn through the data. $D_s = 8.6 \times 10^{-9}$ m²/s was obtained again from the MSD, so τ is the only fit parameter, assuming the value $\tau = 48$ ps.

Comparison with the experimental measurements of ref 14 is hampered by the fact that conditions are different in the experiment, namely $n_{occ} = 2, 4$ at 200 K and 1.5, 2.8 at 250 K. The experimental results under these circumstances and their interpolation or extrapolation to our conditions of $n_{occ} = 3$, 300 K are summarized in Table 4.

From a comparison between extrapolated experimental measurements and the results from our analysis of simulated $S_s(k, \omega)$, we conclude that the diffusion coefficients are in very good agreement, while the jump time constants τ differ. As a consequence, while at small wave numbers almost the same straight line $\Omega = D_s k^2$ is approximated, the experimental limit for $k \rightarrow \infty$ is about two and a half times the value from simulations. Furthermore, the curve from MD clearly approaches the horizontal τ^{-1} from *above*, following a maximum around $k^2 \approx 0.17$ Å^{-2}. This doesn't contradict the experimental results because the neutron scattering gives only four to five points per temperature and loading, too few to determine the shape of the curve. It does contradict eq 34, however. It is possible that the limits of validity of the jump model on which this equation is based have been reached. One might question the reliability of the extrapolation used in the comparison presented here, which is far from being unique. Further simulations and experiments under identical conditions could rule out that source of error. It should be noted, however, that a value of $\tau = 48$ ps would not be consistent with a monotonic variation of jump time on temperature.

Summary

From MD simulation data, we have calculated the self-parts of the van Hove function, the intermediate scattering function, and the dynamic structure factor for the diffusion of methane in ZK4 and silicalite. Values for the self-diffusivities obtained from the decay of the intermediate scattering function at long wavelengths are in good agreement with those from MSD known from previous simulations and the experimental literature. A new approximation is developed for systems where motion occurs by infrequent passages between confined regions in which rapid motion takes place. The approximation is based on the separation of time scales, and it is proved to be reasonable for the self-part of the van Hove function in both ZK-4 and silicalite. For silicalite, the radial dynamic structure factor has also been determined. While for small k the dependence of the line width of the dynamic structure factor upon the wave number k is the same as obtained from quasielastic neutron scattering, there is a significant difference for large k, the reason being still unknown.

Acknowledgment. Stimulating discussions with Dr. Hervé Jobic are gratefully acknowledged. This work was supported by the DFG, Sonderforschungsbereich 294.

References and Notes

(1) Kärger, J.; Ruthven, D. M. *Diffusion in Zeolites and Other Microporous Solids;* Wiley-Interscience: New York, 1992.
(2) Chen, N. Y.; Degan, T. F., Jr.; Smith, C. M. *Molecular Transport and Reaction in Zeolites: Design and Application of Shape Selective Catalysts;* VCH: New York, 1994.
(3) Bell, A. T.; Maginn, E. J.; Theodorou, D. N. Molecular simulation of adsorption and diffusion in zeolites in *Handbook of Heterogeneous Catalysis;* Ertl, G.; Knoezinger, H.; Weitkamp, J.; Eds; VCH: Weinheim, 1997.
(4) Theodorou, D. N.; Snurr, R. Q.; Bell, A. T. Molecular dynamics and diffusion in microporous materials in *Comprehensive Supramolecular Chemistry;* Alberti, G.; Bein, T. Eds; Elsevier Science: Oxford, 1996; Volume 7.
(5) Maginn, E. J.; Snurr, R. Q.; Bell, A. T.; Theodorou, D. N. Simulation of hydrocarbon diffusion in zeolites in *Progress in Zeolite and Microporous Materials*, volume 105 of *Studies in Surface Science and Catalysis;* Chon, H.; Ihm, S. K.; Uh, Y. S., Eds; Elsevier: Amsterdam, 1997.
(6) Hove, L. van *Phys. Rev.* **1954**, *95*, 249.
(7) Hansen, J. P.; McDonald, I. R. *Theory of Simple Liquids;* Academic Press: London, 1986.
(8) Onsager, L. *Phys. Rev.* **1931**, *37*, 405 and *38*, 2265.
(9) Gaub, M. *Molekulardynamische Untersuchungen zur Diffusion von Methan in Zeolithen;* Ph.D. Thesis, Universität Leipzig, 1998.
(10) Fritzsche, S.; Haberlandt, R.; Kärger, J.; Pfeifer, H.; Heinzinger, K. *Chem. Phys.* **1993**, *174*, 229.
(11) June, R. L.; Bell, A. T.; Theodorou, D. N. *J. Phys. Chem.* **1990**, *94*, 8232.
(12) June, R. L.; Bell, A. T.; Theodorou, D. N. *J. Phys. Chem.* **1991**, *95*, 8866.
(13) Hall, P. L.; Ross, D. K. *Mol. Phys.* **1981**, *42*, 673.
(14) Jobic, H.; Bée, M.; Kearley, G. J. *Zeolites* **1989**, *9*, 312.